SCIENCE CHINA
Technological Sciences

• Article •

August 2017 Vol.60 No.8: 1188–1196
doi: 10.1007/s11431-016-0786-7

# A Fourier spectrum-based strain energy damage detection method for beam-like structures in noisy conditions

YANG ZhiBo[1,2], CHEN XueFeng[1*], RADZIENSKI Maciej[2], KUDELA Pawel[2] & OSTACHOWICZ Wieslaw[2,3]

[1] *School of Mechanical Engineering, Xi'an Jiaotong University, Xi'an 710049, China;*
[2] *Institute of Fluid Flow Machinery, Polish Academy of Science, Gdansk 80-231, Poland;*
[3] *Faculty of Automotive and Construction Machinery, Warsaw University of Technology, Warsaw 02-524, Poland*

Received October 20, 2016; accepted January 9, 2017; published online February 14, 2017

In this paper, the Fourier spectrum-based strain energy damage detection method for beam-like structures is proposed based on the discrete Fourier transform. The classical strain energy damage detection method localizes damage by the comparison of the strain energy between the intact and inspected structures. The evaluation of the 2nd-order derivative term in the strain energy plays a crucial part in the comparison. The classical methods are mostly based on a numerical derivative estimation for this term. The numerical derivative, however, introduces additional disturbances into damage indications. To address this problem, a discrete Fourier transform-based strain energy is proposed with the emphasis of enhancing the performance in noisy condition. The validations conducted on the simulated and experimental data show that the developed method is effective enough for composite beam damage detection in noisy environments.

**Fourier spectrum, strain energy (SE), composite beam, noisy condition, damage detection, mode shape**

**Citation:** Yang Z B, Chen X F, Radzienski M, et al. A Fourier spectrum-based strain energy damage detection method for beam-like structures in noisy conditions. Sci China Tech Sci, 2017, 60: 1188–1196, doi: 10.1007/s11431-016-0786-7

## 1 Introduction

Damage detection or assessment is the main task in structural health monitoring (SHM). Based on the damage information provided by SHM system, a reasonable evaluation for the current situation of structures can be made. Among all the SHM technologies, the vibration-based methods are widely used as the vibration signal can be obtained *in-situ* even on-line. Among all the vibration-based methods, the frequency-based and the mode shape-based methods appear to be the most popular ones. The frequency-based methods evaluate damage by the frequency shift before and after the appearance of defects. However, the symmetry of structures may induce the multiple-solution problem [1]. Compared with the frequency-based methods, the mode shape-based technologies can provide the more accurate localization for damage. Thus it is widely employed in applications. During the past decade, many kinds of mode shape-based technologies have been proposed, containing the fractural dimension method [2,3], entropy method [4–6] and so on [7,8].

Strain energy (SE) is one of the most important concepts in the mode shape-based damage detection and fracture mechanics. The corresponding damage assessment methodologies have been widely used in mechanical, civil and the other fields. In fracture mechanics, it is known that the presence of damage changes the SE. The earliest literatures about the SE damage index appear to be refs. [9,10], in which the one-

* Corresponding authors (email: chenxf@mail.xjtu.edu.cn, phdapple@mail.xjtu.edu.cn)

dimensional SE damage index was proposed, and further extended to plate damage detection via dividing the two-dimensional domain into several strips. Shi et al. [11–14] proposed to reveal damage by the change of the modal SE, and constructed the elemental SE. Their method is sensitive to damage, and only the mode shapes and elemental stiffness matrix are required instead of the complete stiffness and mass matrices of the inspected structure. Hu et al. [15–17] extended the SE method to experimental modal analysis and complex structures, and several applications are conducted on composite structures without model update. The effectiveness of the SE-based and the related damage indices have been verified many times [18–23]. However, it should be mentioned that the SE in most of the research works is estimated by numerical derivatives (ND), which makes the current SE-based method unstable in noisy condition. To address this problem, an optimal spatial sampling interval method is proposed by Sazonov et al. [24–26], and a baseline-free damage index is then presented. It is remarkable that the wavelet modal curvature [27–29] estimation is also an effective way to solve the SE estimation problem. Motivated by these works, the Fourier spectrum-based SE damage detection method is proposed with the emphasis of the enhanced performance in noisy environments.

This paper is arranged as follows. Section 2 interprets the theory of the proposed method briefly, and the noise model and crack model are also presented in this part. In Section 3, some comparisons between the presented and the classical methods are demonstrated on a steel beam in noise-free and noisy conditions. In Section 4, the proposed method is further validated via the experiments conducted on composite beams.

## 2 Theory

### 2.1 Strain energy damage detection method

For beam-like structures, the strain energy $u(x)$ yields

$$u(x) = \frac{1}{2}\int_0^L EI\left(\frac{\mathrm{d}^2 w(x)}{\mathrm{d}x^2}\right)^2 \mathrm{d}x, \tag{1}$$

where $E$ is the Young's modulus and $I$ is the moment of the cross-section of beam. The symbol $w$ denotes the deflection of beam, and $x$ is the spatial variable. For a specific mode shape, $w$ can be replaced by the $i$-th mode shape $w_i$. Then the strain energy associated with the $i$-th mode shape is expressed as

$$u_i(x) = \frac{1}{2}\int_0^L EI\left(\frac{\mathrm{d}^2 w_i(x)}{\mathrm{d}x^2}\right)^2 \mathrm{d}x. \tag{2}$$

Consider the beam which is divided into $N$ intervals by $N$–1 nodes, the strain energy associated with element $j$ and the $i$-th mode shape yields

$$u_{ij}(x) = \frac{1}{2}(EI)_j\int_{L_j}^{L_{j+1}}\left(\frac{\mathrm{d}^2 w_i(x)}{\mathrm{d}x^2}\right)^2 \mathrm{d}x, \tag{3}$$

where $L_j$ and $L_{j+1}$ define the interval of the subdivision $j$. In eq. (3), the component $(EI)_j$ has been moved out from the integral as the sub-regions are small enough to keep $(EI)_j$ constant. Based on eq. (3), one can get the energy distribution, which yields

$$F_i(x) = \frac{u_{ij}(x)}{u_i(x)} = \frac{(EI)_j\int_{L_j}^{L_{j+1}}\left(\frac{\mathrm{d}^2 w_i(x)}{\mathrm{d}x^2}\right)^2 \mathrm{d}x}{\int_0^L EI\left(\frac{\mathrm{d}^2 w_i(x)}{\mathrm{d}x^2}\right)^2 \mathrm{d}x}. \tag{4}$$

Eq. (4) is the normalization of elemental strain energy [9,10]. Any singularity in mode shape or the reduction of stiffness will be reflected on the change of $\mathrm{d}^2 w_i(x)/\mathrm{d}x^2$. This can be explained by the damage sensitivity of modal curvature, which is the two-order derivative of mode shape. In the studies of structural healthy monitoring, the change of two-order derivative of mode shape has been proven to be an effective damage index for localization [27,29–31]. Given that the direct measurement of $\mathrm{d}^2 w_i(x)/\mathrm{d}x^2$ is costly, the ND estimation as shown in eq. (5) is usually used

$$\frac{\mathrm{d}^2 w_i(x)}{\mathrm{d}x^2} \approx \frac{w_i(x-\Delta) - 2w_i(x) + w_i(x+\Delta)}{\Delta^2}, \tag{5}$$

where $\Delta$ is the sampling step. However, the noise susceptibility of the ND generates a noise-polluted SE, in which the damage features are easily obscured by disturbances. To address this problem, the discrete Fourier transform-SE (DFT-SE) is proposed in this work, and systematic comparisons will be conducted in Section 3.

It is observed that a priori knowledge about $(EI)_j$ is required in eq. (4). This property is not desirable for a damage index. By assuming that the stiffness factor $EI$ is essentially constant over the length of the beam for both the reference and inspected modes [9,10], eq. (4) can be rearranged to give a damage indication ($DI$) of the change in the flexural rigidity of the sub-region as

$$\begin{aligned} DI &= \mathrm{norm}\left|(EI)_j^r - (EI)_j^d\right| \\ &= \mathrm{norm}\left|\frac{\int_{L_j}^{L_{j+1}}\left(\frac{\mathrm{d}^2 w_i^r(x)}{\mathrm{d}x^2}\right)^2 \mathrm{d}x}{\int_0^L\left(\frac{\mathrm{d}^2 w_i^r(x)}{\mathrm{d}x^2}\right)^2 \mathrm{d}x} - \frac{\int_{L_j}^{L_{j+1}}\left(\frac{\mathrm{d}^2 w_i^d(x)}{\mathrm{d}x^2}\right)^2 \mathrm{d}x}{\int_0^L\left(\frac{d^2 w_i^d(x)}{dx^2}\right)^2 \mathrm{d}x}\right|, \end{aligned} \tag{6}$$

where the superscripts $d$ and $r$ imply "damaged" and "reference/intact", respectively, and "norm" is the normalized function. The occurrence of damage reduces the local stiffness $(EI)_j^d$, the denominator in eq. (6). Therefore, the damage can be localized by the spike in $DI$s. Furthermore, it is observed from the right side of eq. (6) that the change of local stiffness has been described by the integration of curvatures modes, thus the measurement of $EI$ is not required in damage identification.

### 2.2 The DFT-SE damage detection method

Mathematically, the accurate calculation of derivative should be the global rather than local activity as shown in Figure 1. Compared with the ND-based method, the Fourier transform and its properties provide a global estimation scheme for spatial derivatives. Eqs. (7) and (8) are the spatial Fourier transform (FT) and the inverse Fourier transform (IFT) for mode shape $w(x)$

$$W_f(k) = \int_{-\infty}^{+\infty} \mathrm{e}^{-\mathrm{i}kx} w(x)\mathrm{d}x, \tag{7}$$

$$w(x) = \frac{1}{2\pi}\int_{-\infty}^{+\infty} \mathrm{e}^{\mathrm{i}kx} W_f(k)\mathrm{d}k, \tag{8}$$

where $x\in\mathrm{R}$ and $k\in\mathrm{R}$. $W_f(k)$ is the $k$-domain (wavenumber domain) expression of mode shape $w(x)$. The differential property of FT gives the explicit format of the 2nd-order spatial derivative

$$\frac{\mathrm{d}^2 w(x)}{\mathrm{d}x^2} = -\frac{1}{2\pi}\int_{-\infty}^{+\infty} \mathrm{e}^{\mathrm{i}kx} k^2 W_f(k)\mathrm{d}k\,. \tag{9}$$

For finite sampling series, the FT will be replaced by its discrete form DFT (discrete FT) in above equations. Without the loss of generality, assume that $w(x)$ is defined on the interval $[0, 2\pi]$, which is divided by $N$ grid points into $N$–1 components. Eq. (9) is rewritten as

$$\frac{\mathrm{d}^2 w(x)}{\mathrm{d}x^2} = -\frac{h}{2\pi}\sum_k k^2 \mathrm{e}^{\mathrm{i}kx}\sum_x \mathrm{e}^{-\mathrm{i}kx} w(x), \tag{10}$$

where the symbol $h$ depicts the length of each component. In eq. (10), the variables $x$ and $k$ are all bounded and discrete, thus the formulation can be applied in measured data without any technical restrictions. The DFT-based *DI* can be obtained by substitution of eq. (10) into eq. (6). The proposed procedure avoids the use of ND, and hence the noise robustness can be improved. To distinguish the proposed approach with the classical method, they are denoted as DFT-SE and ND-SE, respectively. It is observed from eq. (6) that the material properties $E$ and $I$ are eliminated by means of some reasonable assumptions, and hence the DFT-SE method is capable of detecting defect in absence of a priori about the material properties. On another aspect, the above formulation does not depend on any specific boundary condition.

Besides the above properties, the $k$-domain representation of the mode shape as described in eq. (7) allows the implementation of $k$-domain filtering. In refs. [23,32,33], an iteration algorithm is proposed for modal curvature. The different distributions of damage feature and noise in $k$-domain guarantee that noise can be suppressed by a low-pass filter in $k$-domain, similar with the spatial filtering technology in [34–36]. In this paper, this procedure is briefly introduced with respect to the developed method. In order to choose an appropriate for low-pass filtering, some commonly used windows functions are presented in Figure 2 for comparison. The Nuttall

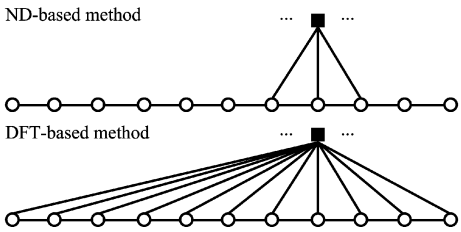


**Figure 1** The differences between the ND-based and the DFT-based estimations for spatial derivatives.

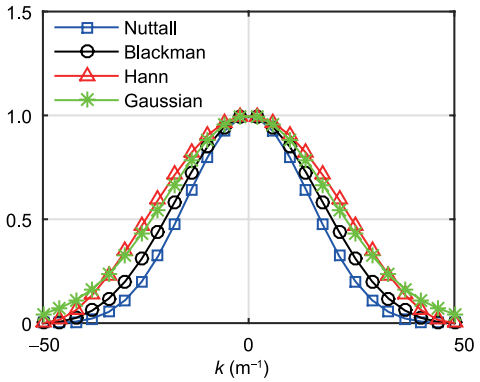


**Figure 2** (Color online) Comparison of different window functions.

window, among all the inspected windows, attenuates the fastest, and hence it is employed in the present algorithm. The main iteration is formulated as

$$W_f^{i+1}(k) = H_b(k) W_f^i(k), \tag{11}$$

where the superscript $i$ depicts the step in iteration as shown in Figure 3, and $\varepsilon$ depicts the convergence error, defined by $\varepsilon = e\|w_x^1\|_\infty$ ($e$ is employed as 1% and $\|\|_\infty$ is the infinite norm). In the following parts, the $k$-domain will be integrated in the presented algorithm without special explanation.

### 2.3 Noise and crack models

Noise is defined as the white Gaussian noise (WGN) by invoking the Matlab function "awgn" (add white Gaussian noise). In numerical validations, crack is modeled by rotational spring following the laws of fracture mechanics. The bending constant of the rotational spring is determined by Castigliano's theorem [6]

$$K_c = \frac{BH^2E}{72\pi\alpha^2 f(\alpha)}, \tag{12}$$

where $B$ is the width, $H$ is the thickness, $\alpha=a/H$, $a$ is the depth of the crack, and $f(\alpha)$ is the dimensionless local compliance function defined by

$$f(\alpha) = 0.6384 - 1.035\alpha + 3.7201\alpha^2 - 5.1773\alpha^3 + 7.553\alpha^4 - 7.332\alpha^5 + 2.4909\alpha^6\,. \tag{13}$$

For multiple-crack conditions, structures are divided by several rotational springs with different damage parameters.

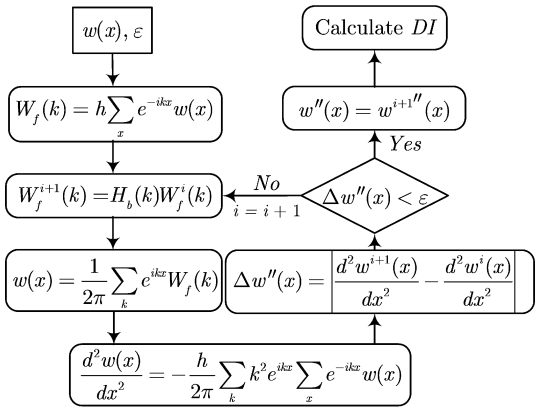


**Figure 3** $k$-domain filtering flowchart.

To be specific, the assembly of a single-cracked beam is illustrated here. Elements are all two-node elements, and thus they have 4 degree of freedoms. Assume the stiffness matrixes of the intact parts are

$$\boldsymbol{K}_{\text{in}}^{L} = \begin{bmatrix} K_{11}^{bb} & K_{12}^{br} & K_{13}^{br} & K_{14}^{bb} \\ K_{21}^{rb} & K_{22}^{rr} & K_{23}^{rr} & K_{24}^{rb} \\ K_{31}^{rb} & K_{32}^{rr} & K_{33}^{rr} & K_{34}^{rb} \\ K_{41}^{bb} & K_{42}^{br} & K_{43}^{br} & K_{44}^{bb} \end{bmatrix}, \tag{14}$$

$$\boldsymbol{K}_{\text{in}}^{R} = \begin{bmatrix} K_{11}^{rr} & K_{12}^{rb} & K_{13}^{rb} & K_{14}^{rr} \\ K_{21}^{br} & K_{22}^{bb} & K_{23}^{bb} & K_{24}^{br} \\ K_{31}^{br} & K_{32}^{bb} & K_{33}^{bb} & K_{34}^{br} \\ K_{41}^{rr} & K_{42}^{rb} & K_{43}^{rb} & K_{44}^{rr} \end{bmatrix}, \tag{15}$$

where the entries in the above matrix are all determined in finite element modeling, and the superscripts $b$ and $r$ depict bending and rotating, respectively. The superscript $L$ and $R$ means left and right, and thus the symbols $\boldsymbol{K}_{\text{in}}^{L}$ and $\boldsymbol{K}_{\text{in}}^{R}$ define the elemental stiffness matrixes of the intact element left and right to the crack. The two intact elements are connected by a rotational spring, which is used to idealize the crack. The stiffness matrix of the rotational spring is given by

$$\boldsymbol{K}_{\text{crack}} = \begin{bmatrix} K_c & -K_c \\ -K_c & K_c \end{bmatrix}. \tag{16}$$

Assemble the stiffness matrixes given in eqs. (14)–(16), one can get

$$\boldsymbol{K} = \begin{bmatrix} K_{11}^{bb} & K_{12}^{br} & K_{13}^{br} & K_{14}^{bb} & 0 & 0 & 0 \\ K_{21}^{rb} & K_{22}^{rr} & K_{23}^{rr} & K_{24}^{rb} & 0 & 0 & 0 \\ K_{31}^{rb} & K_{32}^{rr} & K_{33}^{rr} + K_c & K_{34}^{rb} & -K_c & 0 & 0 \\ K_{41}^{bb} & K_{42}^{br} & K_{43}^{br} & K_{44}^{bb} + K_{11}^{bb} & K_{12}^{br} & K_{13}^{bb} & K_{14}^{br} \\ 0 & 0 & -K_c & K_{21}^{rb} & K_{22}^{rr} + K_c & K_{23}^{rb} & K_{24}^{rr} \\ 0 & 0 & 0 & K_{31}^{bb} & K_{32}^{br} & K_{33}^{bb} & K_{34}^{br} \\ 0 & 0 & 0 & K_{41}^{rb} & K_{42}^{rr} & K_{43}^{rb} & K_{44}^{rr} \end{bmatrix}. \tag{17}$$

The above matrix is the global stiffness matrix composed of two elements. For more complex cases, the above procedure can be easily extended.

## 3 Numerical validations

### 3.1 Numerical model

The basic model is a clamped-clamped composite beam made out of steel. The dimensions of the beam are: length $L$=500 mm, width $B$=25 mm, and thickness $H$=20 mm. Cracks are defined by the following parameters: the distance to the left boundary $L_c$ and depth $d$. All damage scenarios are listed in Table 1: cases #A1 and #A3 are for the single-crack case, and cases #A2 and #A4 are for the multiple-crack case. The numerical model in cases #A1–#A4 contains 700 nodes per order mode shape. Such a dense grid is used to verify the effectiveness of the developed method. The effect of the number of nodes will be discussed at the end of this section.

### 3.2 Damage detection in noise-free conditions

Before the validation in noisy conditions, it is necessary to verify that the present method is sensitive to damage in noise-free condition. Figures 4 and 5 present the *DI*s obtained via ND-SE and DFT-SE for cases #A1 and #A2, respectively. To identify the spike/outlier related to singularity/damage, the thresholds (horizontal lines) defined by the 3$\sigma$ standard [5] are employed in all the figures. Based on the distribution of the SE amplitude, a statistical analysis can be conducted to determine the value of the standard deviation $\sigma$. Thereafter, the thresholds are further determined by the value of 3$\sigma$. Results show that the spikes beyond the thresholds are located exactly at the damage points. Thus, both of the methods are capable of identifying damage in noise-free condition.

### 3.3 Effects of noise

For clarity, the validations for noisy condition are only con-

**Table 1** Damage scenarios used in simulations

| Case | Mode | $L_c$ (mm) | $d$ (mm) | *SNR* (dB) |
|---|---|---|---|---|
| #A1 | 1st–3rd | 300 | 4 | 0 |
| #A2 | 1st–3rd | 200, 300 | 4, 4 | 0 |
| #A3 | 1st | 200 | 4 | 40, 50, 60 |
| #A4 | 1st | 200, 300 | 4, 4 | 40, 50, 60 |

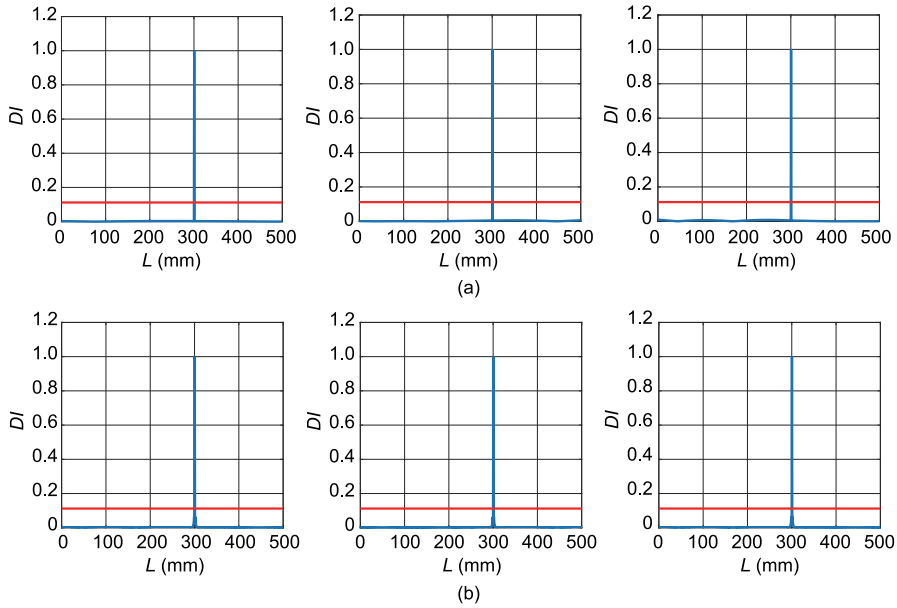


**Figure 4** (Color online) The *DI*s for the single-crack 1st–3rd order mode shapes (from left to right). (a) Based on the ND-SE; (b) based on the DFT-SE.

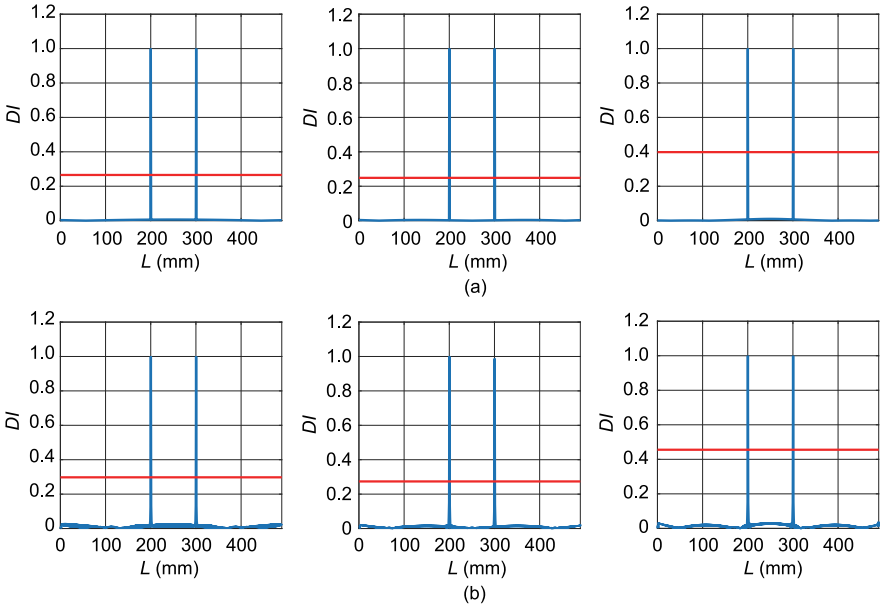


**Figure 5** (Color online) The *DI*s for the multiple-crack 1st–3rd order mode shapes (from left to right). (a) Based on the ND-SE; (b) based on the DFT-SE.

ducted on the 1st-order mode shape. The reference signal and the inspected signal are polluted by two groups of independent noise with the same *SNR*. It should be mentioned that the two groups of independent noise added on the reference and inspected signals also introduce the error similar with model error to some extent. In cases #A3 and #A4, a wide range of noise levels act on the inspected mode shapes, and the associated *DI*s are presented in Figures 6 and 7. For the ND-SE based *DI*s, damage features are fully submerged in the disturbances induced by noise and the numerical error generated in numerical approximations. However, the *DI* performs better when it is combined with the DFT-SE. Noise is suppressed according to the presented algorithm and the *k*-domain filtering, and the characteristics of damage are also retained. In these figures, the outliers identified by thresholds indicate the damage singularities accurately. An additional outlier is wrongly identified in the 40 dB case in Figure 7 by accident, but most of the noise-induced peaks are lower than the threshold defined by $3\sigma$.

### 3.4 Effects of node density

The effect of node density is a complex issue as discussed in refs. [27,29,37]. To choose an appropriate node density and test the corresponding effects are the aims of this section. For

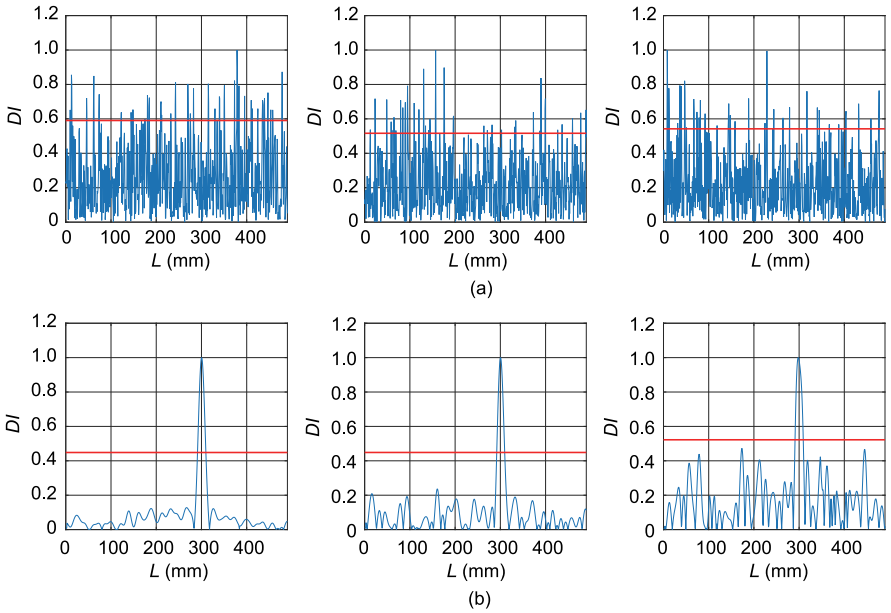


**Figure 6** (Color online) The noise immunity test via case #A3 at noise levels $SNR$=60, 50, 40 dB (from left to right). (a) *DI*s based on the ND-SE; (b) *DI*s based on the DFT-SE.

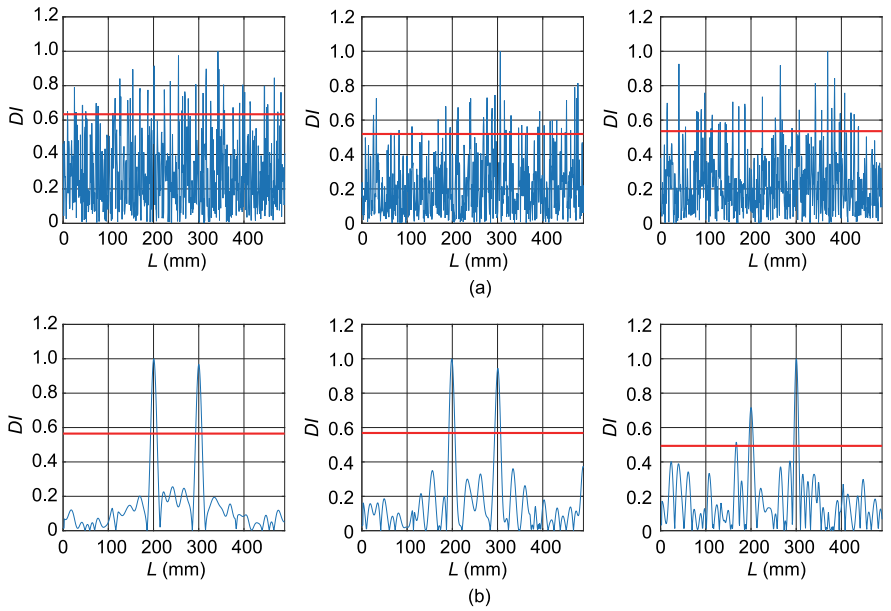


**Figure 7** (Color online) The noise immunity test via case #A4 at noise levels $SNR$=60, 50, 40 dB (from left to right). (a) *DI*s based on the ND-SE; (b) *DI*s based on the DFT-SE.

the mentioned purpose, a single-crack ($L_c$=300mm, $d$=4mm, $SNR$=50 dB) 1st-order mode shape is employed as the basic model, and four different groups of mode shape data are employed. These data are comprised of 300, 150, 50 and 30 nodes, respectively. The associated *DI*s is demonstrated in Figure 8. Similar with the conclusion obtained in Section 3.3, the ND-SE based method does not perform well in noisy condition. The sparsification does not improve the performances of this method. By contrast, the present method features the damage clearly in all four samples. In the case of 50-node and 30-node results, one can see that spikes shift a little as the consequence of sparsification. The above validations also present that the grid density (44 or 39 points) to be used in experiments is suitable for the developed method.

## 4 Experimental validations

The specimens are made out of 24-layered glass-fiber reinforced plastic (GFRP) with unidirectional impregnated fibers and the [0°/60°/–60°] lay-up. The length $L$=250mm, width

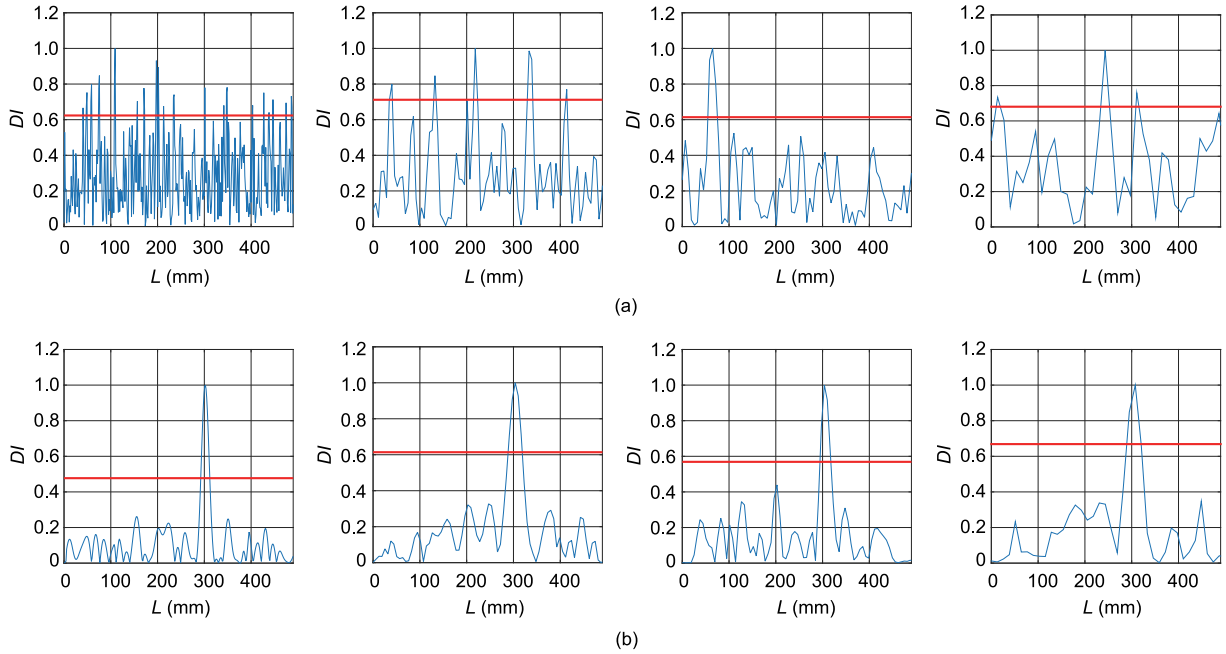


**Figure 8** (Color online) Comparison of node density effects. (a) *DI* based on the ND-SE; (b) *DI* based on the DFT-SE. The corresponding number of nodes: 300, 150, 50, 30 (from left to right) for each row.

$B$=25 mm, thickness $H$=5.28 mm, and the boundary condition is set as clamped-clamped. The data used in validations are obtained from the benchmark provided by Katunin et al. [20,38,39]. Three groups of data are selected in this work and the details are listed in Table 2, Res01 contains the 1st–4th mode shapes for the intact beam; Res05 contains the 1st–4th mode shapes for the beam with a single crack located about 150 mm away from the left edge; Belka1 contains the 1st–3rd mode shapes for the beam with two cracks located about 50 and 119 mm away from the left edge. For more details of the experiment setup and parameters, the readers are suggested to refer to refs. [20,38,39]. In the following validations, the data Res01 is adopted as the reference signal for the other two groups of mode shapes.

The first validation is based on the comparison between data Res01 and Res05. The results obtained by the ND-SE and DFT-SE based *DI*s are presented in Figure 9. In this case, both of the methods perform well although a false outlier appears in the result obtained by the ND-SE based *DI* for the 4th-order mode shape. The satisfying performances of these two methods can be attributed to the strong damage feature contained in the measured data. In the further investigation, two groups of independent noise will be introduced into Res01 and Res05 to simulate a more severe noisy environment. Before that, the multiple-crack case is investigated.

**Table 2** Damage scenarios in experiments

| Data name | $L_c$ (mm) | Mode shape |
|---|---|---|
| Res01 | – | 1st–4th |
| Res05 | 150 | 1st–4th |
| Belka1 | 50,119 | 1st–3rd |

Res01 and Belka1 are adopted in multiple-crack detection, and the *DI*s obtained by ND-SE and DFT-SE based methods are demonstrated in Figure 10. The damage features are submerged into the modal trends in the results given by the ND-SE based method. However, the developed method reveals the two damage locations quite accurately for different mode shapes. Compared with the distinct damage indicator shown in Figure 9, the indicators shown in Figure 10 are rather blurred. This problem can be explained by the benchmark data itself, as the damage singularities are very weak, which can be found in the damage identification presented in refs [20,38,39].

## 5 Conclusions

The Fourier spectrum-based strain energy damage detection method is proposed in this paper based on the DFT. Simulations and experimental studies show the effectiveness of the proposed method in noisy conditions. As described in formulas, the presented method requires the mode shape measured from the intact structure to serve as baseline data. Thus the model update or modification may affect the performance of the proposed algorithm. This issue is not further discussed in this work. Instead, some groups of artificial noise are introduced into the baseline and inspected signals to simulate the influence of noise and model error. Results show that the presented method is capable of damage detection in noisy environments. If the damage occurs at/near the nodal points of

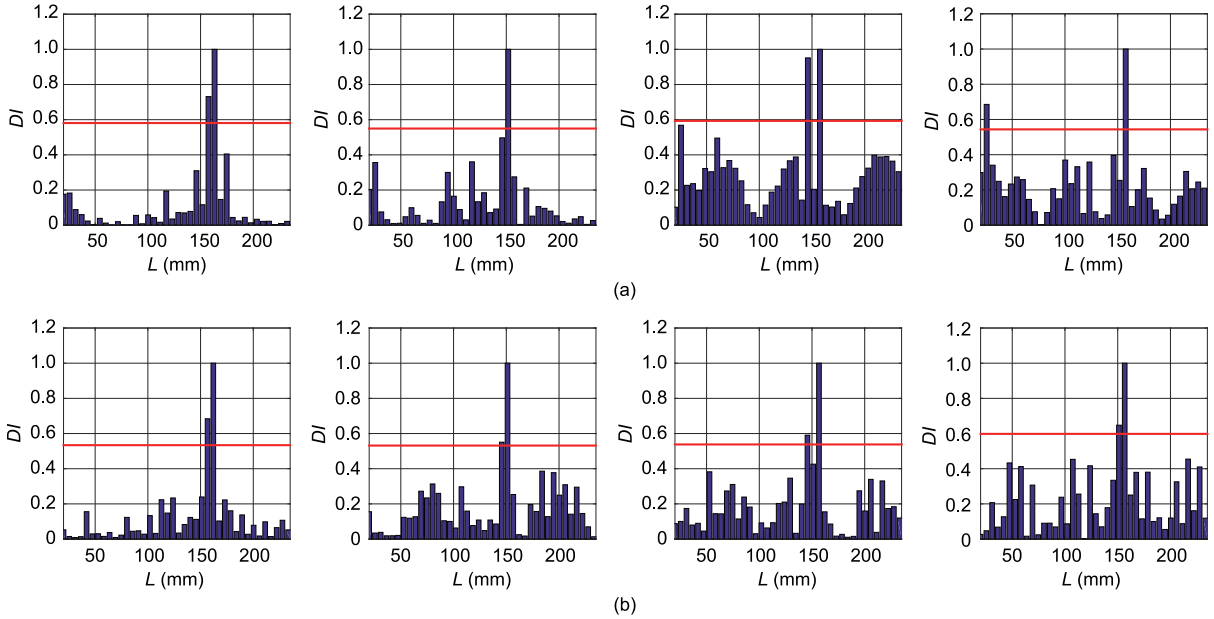


**Figure 9** (Color online) Damage localization for single-crack structure. (a) ND-SE based *DI*s for the 1st–4th mode shapes; (b) DFT-SE based *DI*s for the 1st–4th mode shapes.

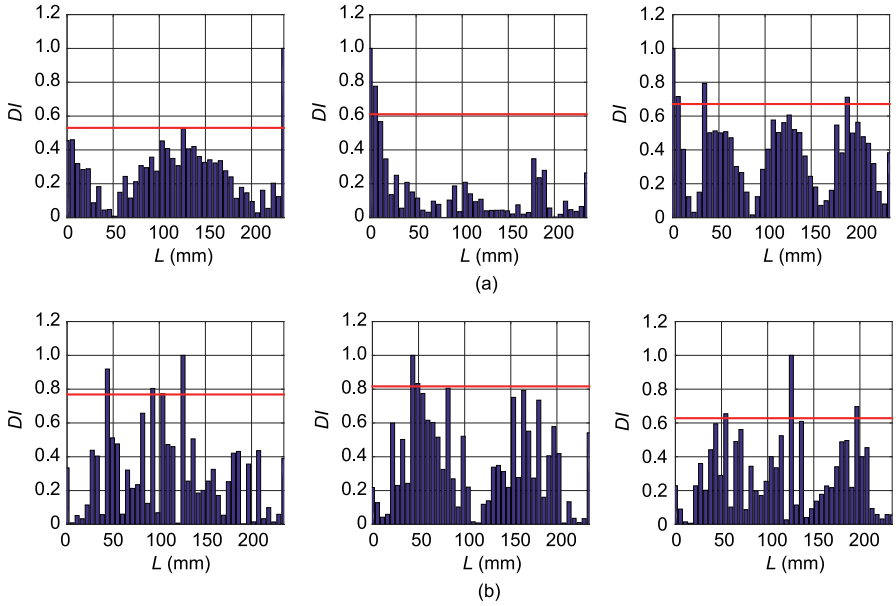


**Figure 10** (Color online) Damage localization for multiple-crack structure. (a) ND-SE based *DI*s of the 1st–3rd mode shapes; (b) DFT-SE based *DI*s of the 1st–3rd mode shapes.

the inspected mode shape, the developed method cannot present a satisfying result. To address this problem, more mode shapes can be involved into damage assessment.

*This work was supported by the National Natural Science Foundation of China (Grant Nos. 51405369 & 51421004), the National Key Basic Research Program of China (Grant No. 2015CB057400), the National Natural Science Foundation of Shaanxi Province (Grant No. 2016JQ5049), and the Postdoctoral Science Foundation of Shaanxi Province. Special acknowledgements should be addressed to Prof. A. Katunin, who shared the benchmark in the website.*

1 Yang Z, Chen X, Yu J, et al. A damage identification approach for plate structures based on frequency measurements. Nondestr Test Eval, 2013, 28: 321–341
2 Bai R, Cao M, Su Z, et al. Fractal dimension analysis of higher-order mode shapes for damage identification of beam structures. Math Problems Eng, 2012, 2012: 1–16
3 Yang Z, Chen X, Tian S, et al. Multiple damages detection in beam based approximate waveform capacity dimension. Struct Eng Mech, 2012, 41: 663–673
4 Yang Z, Chen X, Jiang Y, et al. Generalised local entropy analysis for crack detection in beam-like structures. Nondestr Test Eval, 2014, 29: 133–153
5 Yang Z B, Chen X F, Xie Y, et al. Hybrid two-step method of damage

detection for plate-like structures. Struct Control Health Monit, 2016, 23: 267–285
6 Yang Z B, Chen X F, Xie Y, et al. The hybrid multivariate analysis method for damage detection. Struct Control Health Monit, 2016, 23: 123–143
7 Zhang C L, Li B, Yang Z B, et al. Crack location identification of rotating rotor systems using operating deflection shape data. Sci China Tech Sci, 2013, 56: 1723–1732
8 Chen B Q, Zhang Z S, Zi Y Y, et al. A pseudo wavelet system-based vibration signature extracting method for rotating machinery fault detection. Sci China Tech Sci, 2013, 56: 1294–1306
9 Cornwell P, Doebling S W, Farrar C R. Application of the strain energy damage detection method to plate-like structures. J Sound Vib, 1999, 224: 359–374
10 Doebling S W, Hemez F M, Peterson L D, et al. Improved damage location accuracy using strain energy-based mode selection criteria. AIAA J, 1997, 35: 693–699
11 Shi Z Y, Law S S, Zhang L M. Structural damage localization from modal strain energy change. J Sound Vib, 1998, 218: 825–844
12 Law S S, Shi Z Y, Zhang L M. Structural damage detection from incomplete and noisy modal test data. J Eng Mech, 1998, 124: 1280–1288
13 Shi Z Y, Law S S, Zhang L M. Structural damage detection from modal strain energy change. J Eng Mech, 2000, 126: 1216–1223
14 Shi Z Y, Law S S, Zhang L M. Improved damage quantification from elemental modal strain energy change. J Eng Mech, 2002, 128: 521–529
15 Hu H, Wu C, Lu W J. Damage detection of circular hollow cylinder using modal strain energy and scanning damage index methods. Comp Struct, 2011, 89: 149–160
16 Hu H, Wu C. Development of scanning damage index for the damage detection of plate structures using modal strain energy method. Mech Syst Signal Process, 2009, 23: 274–287
17 Hu H, Wang B T, Lee C H, et al. Damage detection of surface cracks in composite laminates using modal analysis and strain energy method. Composite Struct, 2006, 74: 399–405
18 Xiang J, Matsumoto T, Long J, et al. A simple method to detect cracks in beam-like structures. Smart Struct Syst, 2012, 9: 335–353
19 Xiang J W, Matsumoto T, Wang Y X, et al. A hybrid of interval wavelets and wavelet finite element model for damage detection in structures. CMES-Comp Model Eng Sci, 2011, 81: 269–294
20 Katunin A, Dragan K, Dziendzikowski M. Damage identification in aircraft composite structures: A case study using various non-destructive testing techniques. Composite Struct, 2015, 127: 1–9
21 Katunin A, Przystałka P. 1730. Automated wavelet-based damage identification in sandwich structures using modal curvatures. J Vibroeng, 2015, 17: 2977–2986
22 Katunin A, Przystałka P. Damage assessment in composite plates using fractional wavelet transform of modal shapes with optimized selection of spatial wavelets. Eng Appl Artif Intell, 2014, 30: 73–85
23 Yang Z B, Radzienski M, Kudela P, et al. Fourier spectral-based modal curvature analysis and its application to damage detection in beams. Mech Syst Signal Process, 2017, 84: 763–781
24 Sazonov E, Klinkhachorn P. Optimal spatial sampling interval for damage detection by curvature or strain energy mode shapes. J Sound Vib, 2005, 285: 783–801
25 Sazonov E S, Klinkhachorn P, Gangarao H V S, et al. Fuzzy logic expert system for automated damage detection from changes in strain energy mode shapes. Nondestr Test Eval, 2002, 18: 1–20
26 Sazonov E S, Klinkhachorn P, Halabe U B, et al. Non-baseline detection of small damages from changes in strain energy mode shapes. Nondestr Test Eval, 2002, 18: 91–107
27 Cao M S, Xu W, Ren W X, et al. A concept of complex-wavelet modal curvature for detecting multiple cracks in beams under noisy conditions. Mech Syst Signal Process, 2016, 76-77: 555–575
28 Xu W, Cao M, Ostachowicz W, et al. Two-dimensional curvature mode shape method based on wavelets and Teager energy for damage detection in plates. J Sound Vib, 2015, 347: 266–278
29 Cao M, Xu W, Ostachowicz W, et al. Damage identification for beams in noisy conditions based on Teager energy operator-wavelet transform modal curvature. J Sound Vib, 2014, 333: 1543–1553
30 Fan W, Qiao P. A strain energy-based damage severity correction factor method for damage identification in plate-type structures. Mech Syst Signal Process, 2012, 28: 660–678
31 Abdel Wahab M M. Effect of modal curvatures on damage detection using model updating. Mech Syst Signal Process, 2001, 15: 439–445
32 Yang Z B, Radzienski M, Kudela P, et al. Scale-wavenumber domain filtering method for curvature modal damage detection. Composite Struct, 2016, 154: 396–409
33 Yang Z B, Radzienski M, Kudela P, et al. Two-dimensional modal curvature estimation via Fourier spectral method for damage detection. Composite Struct, 2016, 148: 155–167
34 Tondreau G, Deraemaeker A. Automated data-based damage localization under ambient vibration using local modal filters and dynamic strain measurements: Experimental applications. J Sound Vib, 2014, 333: 7364–7385
35 Tondreau G, Deraemaeker A. Local modal filters for automated data-based damage localization using ambient vibrations. Mech Syst Signal Process, 2013, 39: 162–180
36 Tondreau G, Deraemaeker A. Experimental localization of small damages using modal filters, in Special Topics in Structural Dynamics. New York: Springer, 2013. 585–591
37 Cao M, Radzieński M, Xu W, et al. Identification of multiple damage in beams based on robust curvature mode shapes. Mech Syst Signal Process, 2014, 46: 468–480
38 Katunin A. Nondestructive damage assessment of composite structures based on wavelet analysis of modal curvatures: State-of-the-art review and description of wavelet-based damage assessment benchmark. Shock Vib, 2015, 2015: 1–19
39 Katunin A. Diagnostics of Composite Structures Using Wavelets. Gliwice: Department of the Institute for Sustainable Technologies, 2015